arXiv:1403.8124v2 [cond-mat.soft] 1 Apr 2014

# Penetration depth scaling for impact into wet granular packings

T.A. Brzinski III,[1] J. Schug,[1,2] K. Mao,[1,3] and D.J. Durian[1]

[1] *Department of Physics & Astronomy, University of Pennsylvania, Philadelphia, PA 19104, USA*
[2] *William Penn Charter School, Philadelphia, PA 19144, USA*
[3] *The Haverford School, Haverford, PA 19041, USA*

(Dated: April 2, 2014)

We present experimental measurements of penetration depths for the impact of spheres into wetted granular media. We observe that the penetration depth in the liquid saturated case scales with projectile density, size, and drop height in a fashion consistent with the scaling observed in the dry case, but that penetration depths into saturated packings tend to be smaller. This result suggests that, for the range of impact energies observed, the stopping force is set by static contact forces between grains within the bed, and that the presence of liquid serves, primarily, to enhance these contact forces. The enhancement to the stopping force has a complicated dependence on liquid fraction, accompanied by a change in the drop-height dependence, that must be the consequence of accompanying changes in the conformation of the liquid phase in the interstices.

PACS numbers: 45.70.-n, 47.57.Gc, 83.80.Fg, 81.70.Bt

## I. INTRODUCTION

Many of the materials of interest in geophysics, mining, engineering, and industry are granular in nature. Most physics research has focused on dry, noncohesive grains, but in many situations grains are wet, either by circumstance or design. Introducing liquid to a granular packing results in dramatic, qualitative changes to its rheology, as can be observed when comparing the sand above and below the tide lines at the beach. Experimental studies of wet granular rheology have generally focused on static or low strain-rate bulk measurements [1, 2]. Measurements of angle of repose and angle of stability [3–5], tensile strength [6, 7], and yield under uniaxial compression [8], all reveal a similar non-monotonic dependence on the fraction of pore space, $S$, occupied by the liquid phase: the stress at which a packing fails increases with $S$ for small $S$, and decreases as $S$ approaches unity, but exhibits little dependence for intermediate liquid fractions. The liquid fraction dependence of the repose angle in the limit of vanishing $S$ has been shown to be consistent with the balance between stresses due to the weight of the packing and the stress provided by liquid bridges between grains [5]. Direct imaging of liquid conformation for small liquid fractions, in parallel with measurements of tensile strength, revealed that tensile strength saturates as the number of liquid bridges in the packing reaches its maximum [7]. Thus statics experiments have shown that cohesive forces which arise from surface tension strengthen the packing, but as we consider dynamics there must also be viscous interactions between moving grains, and even the liquid inertia must become important for fast dynamics. Unfortunately such dynamical effects have been difficult to characterize with conventional rheometric techniques, which are frustrated by shear localization.

An alternative approach which has been successful for dry packings [9] is to study impact. A projectile falling from rest through height $h$ above a granular packing will come to rest after penetrating the packing to depth $d$, so the average force exerted by the packing on the projectile, by conservation of energy, is $\langle F\rangle = mgH/d$, where $m$ is the projectile mass, $g$ is gravity, and $H = h + d$ is the total drop distance. The full scaling behavior of the penetration depth, $d$, for spherical projectiles of diameter $D$, free falling from rest onto a bed of hard, dry, noncohesive grains was explored in [10–12], and shown to have the form

$$d = (0.14/\mu){\rho_n}^{1/2} D^{2/3} H^{1/3} \ . \tag{1}$$

Here $\rho_n = \rho_p/\rho_g$, where $\rho_g = \phi\rho_{gm}$ is the mass density of the granular media, $\phi$ is the volume fraction of grains in the packing, $\rho_{gm}$ is the mass density of the grain material, and $\rho_p$ is the density of the projectile; $\mu = \tan\theta_R$ is the internal coefficient of friction for the dry granular material, where $\theta_R$ is the angle of repose. Volfson and Tsimring [13] showed that the observed $H^{1/3}$ scaling is consistent with a modified Poncelet equation of motion,

$$ma = -mg + kz + bv^2 \tag{2}$$

where $m$ is the projectile mass, $g = 9.8$ m/s$^2$, and $\{z, v, a\}$ are respectively the projectile depth, velocity, and acceleration. The empirical coefficients $k$ and $b$ depend on materials parameters. Eq (2) may be solved analytically for the penetration depth [14, 15]; the result is consistent with Eq. (1), but the mapping is not exact [15, Fig.5].

Though Eq. (1) has yet to be rigorously tested and modified in order to describe wet materials, there have recently been several experimental studies of impact in wetted grains [16–18]. Marston et al. [16] found that, for large impact velocities and small $S$, penetration depths can be greater than in the dry case. Only Marston et al. have observed this increase in penetration depth: in all other cases, and for all liquid saturations, the penetration depth has been smaller than for a dry packing. Furthermore, in both Refs. [16] and [18] there is no appreciable change in the $H$-dependence of the penetration

depth on $S$. Nordstrom et al. [17] study a system of grains fully submerged in a low-viscosity fluid. The authors again reproduce the $H^{1/3}$ scaling, and demonstrate that $b$ is proportional to the average mass density of the grain-fluid mixture.

Here we conduct a series of impact experiments in order to explicitly test the applicability of Eq. (1) for impacts onto granular packings as we vary liquid content from the dry case, $S = 0$, to the fully saturated $S = 1$ case. We recover a dependence of penetration depth on $S$ that is qualitatively similar to that in Ref. [18], but also find that the presence of liquid in the packing changes the $H$-scaling of Eq. (1). This is the first observation of this effect, which is non-monotonic in $S$. For both $S = 0$ and 1 we recover $H^{1/3}$ scaling, but for intermediate values, we observe a higher-power relation. This power reaches a maximum between $S = 0.28$ and 0.43, and has a local minimum around $S = 0.56$. We also pay particular attention to the $S = 1$ case, where we vary drop height, projectile size, and material density, and find good agreement with Eq. (1), only with a reduced coefficient. Because there are no liquid bridges between grains at $S = 1$, one might expect hydrodynamic interactions to be the only cause for the reduced coefficient. We find that this cannot be the case, as the effect of the interstitial fluid is stronger for a less viscous fluid. We propose that dilatancy-induced perturbation of the liquid surface, and the resulting stress due to surface tension, account for the difference.

## II. MATERIALS AND METHODS

In the present work, all data are for impacts into packings of spherical glass grains wetted either by water or mineral oil (McMaster-Carr Supply Company, Light Viscosity). For all water-wetted samples, an open-topped, plastic cylinder, 10.8 cm in diameter, is filled with 515 $\mu$m diameter glass spheres (Potters Industries, stock number P-0230), then water is poured into the granular packing at a rate slow enough that no water accumulates at the surface. Once the level of the water is above the top of the grains, more sand is added, and the process repeated until there is fully saturated sand just above the lip of the container. Note that all samples wetted with water are fully saturated, such that $S = 1$. For all oil-wetted samples, the oil and 365 $\mu$m diameter glass spheres (Potters Industries, stock number P-0170) are stirred together with a wooden spatula until the material has no clumps, and is homogenous to the eye. The wetted granular mixture is then used to fill the plastic cylinder to above the lip, then leveled by scraping excess material off the top such that the surface of the granular material is flush with the top of the container. The mineral oil has a viscosity of 32 times that of water, half the surface tension of water, and is 0.85 the density of water. The masses of oil and grains in each mixture are measured, and used to characterize the mixtures by their liquid saturation, $S$, which we vary as indicated in Table I.

The projectiles are spherical and made of wood, or of various plastics or metals, in order to vary the density. We vary the diameter and density for impacts onto water- and oil-wetted packings as reported in Table I. All projectiles have a small square rod protruding perpendicular to the projectile surface. The rod is capped with a piece of ferrous metal. This metal tip is used to suspend the sphere from an electromagnet centered above the cylindrical container. We measure the height above the granular surface, $h$, from which the projectile is to be dropped with a height gauge and cathetometer. The projectile is released by turning off the electromagnet, allowing the projectile to fall and impinge upon the granular surface at impact speed $\sqrt{2gh}$. We measure the total distance through which the projectile falls, $H$, again with the height gauge. The penetration depth is then given by the difference $d = H - h$.

## III. RESULTS

### A. Fully Saturated

We begin by examining the case of fully saturated packings, $S = 1$, in which the interstitial volume is occupied exclusively by either water or mineral oil. In this case there are no interstitial air/liquid interfaces, and thus no cohesive interparticle forces due to surface tension. For comparison, data are also included for impact into dry grains. Measurements of penetration depth, $d$, for impacts of multiple projectiles dropped from a range of heights are plotted in Fig. 1 in order to compare with Eq. (1). The data are plotted against each of our control parameters in turn: (a) the total drop distance, $H$; (b) projectile diameter, $D$; (c) normalized projectile density, $\rho_n$. In Fig. 1(a), the penetration depth is normalized according to the $\rho_n$ and $D$ scaling predicted by Eq. (1), yielding $dD^{-2/3}\rho_n^{-1/2}$. Surprisingly, the penetration depth is not only collapsed by this normalization, but also scales, as in the dry case, as $H^{1/3}$ for each liquid-saturated packing. Following the same prescription for Fig. 1(b), the penetration depth is normalized by the expected $H$ and $\rho_n$ dependence to yield $dH^{-1/3}\rho_n^{-1/2}$. While projectile size and density were varied only in the water saturated case, we find again that the normalization collapses the data, and that the projectile size dependence is consistent with the $D^{2/3}$-scaling of Eq. (1). Likewise, in Fig. 1(c) the data are collapsed by the normalization $dH^{-1/3}D^{-2/3}$, and demonstrate $\rho_n^{1/2}$ scaling, consistent with Eq. (1).

To coalesce Figs. 1(a-c), we plot penetration depth, $d$ as a function of ${\rho_n}^{1/2}D^{2/3}H^{1/3}$ in Fig. 1(d). We observe that all three data sets collapse onto lines of slope 1, reflecting that the penetration depth scaling for impacts into liquid saturated grains is consistent with Eq. (1). However the constant of proportionality

TABLE I: Material properties for the different bulk granular materials used, as well as the projectile diameters, projectile materials, projectile densities and liquid saturations tested for each material. Experiments conducted with water are by J.S. and T.A.B., all others are by K.M. and T.A.B.

..

| Fluid | $\eta_f$ [cP] | $\rho_f$ [g/cm$^3$] | $\sigma$ [dyn/cm] | $d_g$ [$\mu$m] | $S$ | $D$ [cm] | $\rho_p$ [g/cm$^3$] | projectile material |
|---|---|---|---|---|---|---|---|---|
| Air | 0.019 | 0.0013 | N/A | 365 | 0 | 2.54 | 0.464 | wood |
| Oil | 29 | 0.85 | $32.5 \pm 2.5$ | 365 | 0 - 1 | 2.54 | 0.464 | wood |
| Water | 0.89 | 1 | 72 | 515 | 1 | 1.27 - 5.08 | 0.685 | wood |
| Water | 0.89 | 1 | 72 | 515 | 1 | 2.54 | 0.685 - 7.762 | miscellaneous |

is different for each packing preparation: 0.14 for dry grains, 0.091 for oil-saturated grains, and 0.044 for water-saturated grains. Thus, Eq. (1) captures the full dependence of $d$ on total drop distance $H$, projectile size $D$, and material density $\rho_n$ for both dry and saturated packings, but the empirical prefactor is dependent on some property or properties of the liquid: viscosity, surface tension, or fluid density.

The scaling behavior of the data in Fig. 1d for the liquid-saturated packings is the same as for dry packings, except for a numerical pre factor, which suggests that Eqs.(1,2) are relevant. But since they include neither viscosity nor surface tension terms, these forces seem unlikely to play a role. The participation of viscous forces is further counterindicated by the fact that penetration is greater for oil than for water, while the viscosity of oil is more than an order of magnitude greater than that of water. Also, the grain size used for oil saturated grains is smaller, which should result in larger relative viscous forces.

Unlike viscosity, the role of fluid density can be argued from Eq. (1) and the materials dependence of the coefficients in Eq. (2). There are two effects. First, $bv^2$ represents inertial drag. So $b$ should be proportional to the total mass density $\phi\rho_{gm} + (1-\phi)\rho_f$ of the grain plus fluid mixture. Nonzero $\rho_f$ gives a larger inertial drag and hence a smaller penetration. Since Eq. (2) cannot be mapped onto Eq. (1), we suppose that this effect may be accounted for by modifying the granular medium density in Eq. (1) from $\rho_g = \phi\rho_{gm}$ to $\rho_g = \phi\rho_{gm}[1 + (1/\phi - 1)\rho_f/\rho_{gm}]$. Second, $kz$ represents quasistatic friction due to gravitationally loaded grain-grain contacts [14]. Interstitial fluid unloads these contacts due to buoyancy, and this should cause a smaller quasistatic stopping force and hence a larger penetration. Thus we expect $k \propto \mu(\rho_{gm} - \rho_f)$, and suppose this may be accounted for by modifying the effective friction coefficient in Eq. (1) to $\mu(1 - \rho_f/\rho_{gm})$. The repose angles of dry and submerged grains differ by only a couple degrees, so $\mu$ itself is nearly unaltered [19]. Altogether then, the effect of nonzero fluid density would be to change the numerical coefficient of Eq. (1) from 0.14 to $0.14/[(1-\rho_f/\rho_{gm})\sqrt{1 + (1/\phi - 1)\rho_f/\rho_{gm}}]$. This yields 0.19 and 0.21 for oil- and water-saturated packings, respectively, which would mean that the reduced friction beats the increased inertial drag, giving deeper penetration than for dry grains. However we find shallower penetrations, with measured coefficients of 0.091 and 0.044, so the expected density effect is opposite to that observed. While the density effect thus cannot explain our results, it could play a role in the deeper penetrations observed in Ref. [16].

Finally, the static packing is not cohesive in the case of $S = 1$, so it seems unlikely that surface tension could be responsible for the reduced penetration depths demonstrated in Fig. 1. However, the surface tension of water is significantly higher than that of mineral oil, consistent with deeper penetration into oil-saturated packings than into water-saturated packings. It may be that impact stimulates surface tension-driven cohesion in the bed. One possible mechanism is suction as a result of a reduction of pore pressure during impact due to dilatancy and capillary action at the packing boundary. This mechanism would most likely modify the friction-like term of the stopping force by enhancing contact forces between grains, but if this is the case, it is surprising that $d$ demonstrates scaling consistent with Eq. (1). Capillarity with the projectile could also arise. The only way to entirely eliminate such capillarity effects would be to conduct impact experiments with an entirely submerged system.

### B. Partially Saturated

Next we observe the effects of varying the amount of interstitial liquid by conducting impacts onto packings which are partially saturated with oil. Penetration depth, $d$, as a function of total drop distance, $H$, is plotted in Fig. 2 for spheres dropped onto granular packings of different liquid saturations, $S$. Spheres dropped onto packings of dry grains penetrate as Eq. (1), in agreement with previous experiments. *All* spheres dropped onto packings of wet grains stop at a depth shallower than for spheres falling through the same total distance into dry packings, indicating that a wet packing will always exert a stopping force greater than in the dry case. Fig. 3 shows $d$, as a function of $S$ for several drop heights, where $d$ is normalized according to Eq. (1). We see the same general behavior for all $H$: the reduced penetration depths are

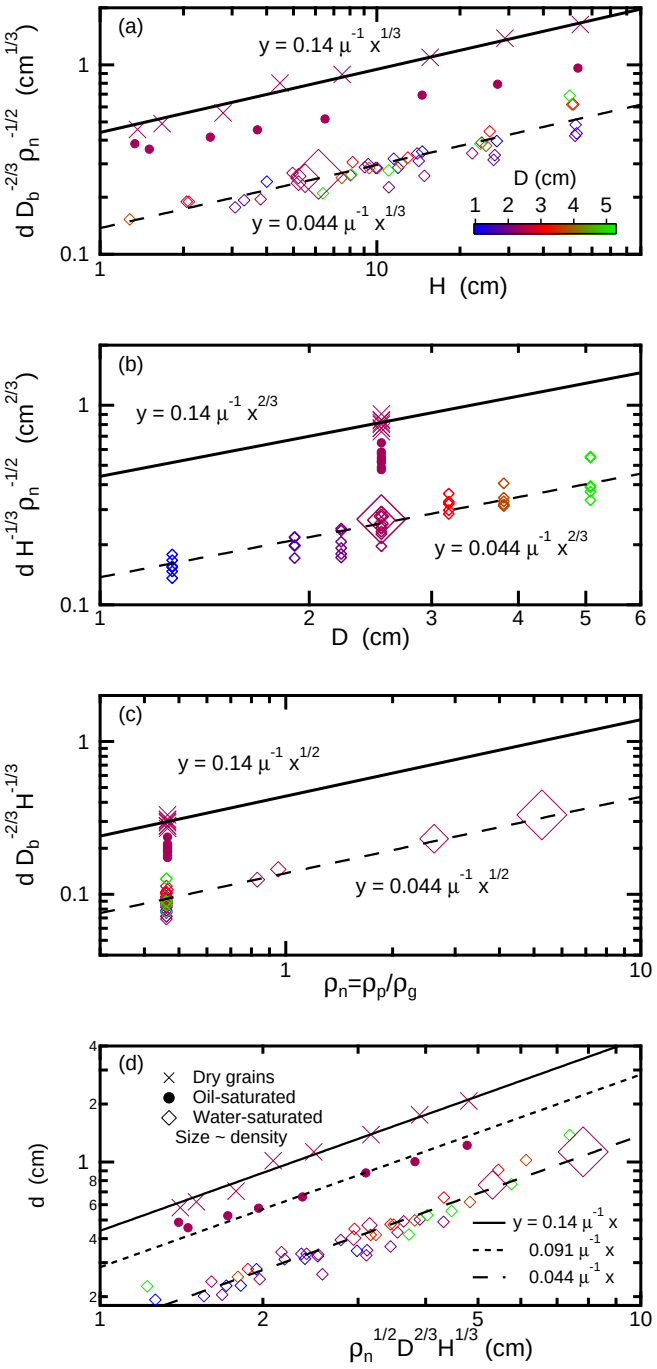


FIG. 1: (Color online) Data for spherical projectiles of diameter 1.27, 1.91, 2.22, 2.54, 3.18, 3.81, and 5.08 cm (indicated by color), and density 0.685, 1.23, 1.41, 3.86, and 7.76 g/mL (indicated by symbol size), dropped onto packings of dry (crosses) and saturated grains using each preparation (circles and diamonds for oil-saturated and water-saturated respectively). The solid lines are Eq. (1). a) $dD^{-2/3}\rho_n^{-1/2}$ plotted against total drop distance, $H$. The dashed line is a power law with a power of 1/3. b) $dH^{-1/3}\rho_n^{-1/2}$ plotted against projectile diameter, $D$. The dashed line is a power law with a power of 2/3. c) $dH^{-1/3}D^{-2/3}$ plotted against $\rho_n$. The dashed line is a power law with a power of 1/2. d) $d$ plotted against $\rho_n^{1/2}D^{2/3}H^{1/3}\mu^{-1}$. The dashed line is a fit of the water-saturated data to a proportionality.

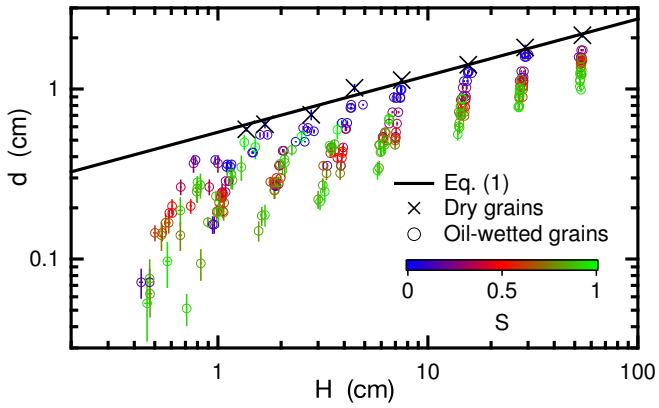


FIG. 2: (Color online) Penetration depth, $d$, plotted against total drop distance, $H$, for spheres of diameter 2.54 cm and density 0.464 g/mL, dropped onto a bed of spherical glass beads, both dry (black crosses), and wetted by oil (circles), with liquid saturations as indicated by color.

non-monotonic with $S$. There is a rapid initial reduction of penetration depth until $S = 0.2$, followed by a range of $S$-values for which $d$ does not change significantly. At $0.4 \leq S \leq 0.55$, $d$ increases, then subsequently decreases at $S \geq 0.55$. Finally, as the packing approaches submersion at $S = 1$, we see $d$ increase once more.

Note that in Fig. 3, as in Fig. 1, normalizing according to Eq. (1) collapses the data for both $S = 0$ and $S = 1$. However, for intermediate values of $S$ the data do not collapse, and the quality of the collapse demonstrates a strong, non-linear $S$-dependence. The dependence of penetration depth on $H$ becomes stronger than a 1/3 power law as $S$ increases from 0, and $d$ initially decreases. This effect reaches its maximum by $S = 0.2$. Between $S = 0.4$ and 0.5, the effect becomes very small, with $d$ once again approaching $H^{1/3}$ scaling. The effect becomes more pronounced for $0.6 \leq S \leq 0.9$, before vanishing again as $S \to 1$.

While there is a temptation to relate this behavior to a taxonomy of liquid conformation, the lack of data on the conformation phase-space in 3-D renders such statements purely speculative. That said, some excellent data on liquid distribution for $S \leq 0.3$ was presented in Ref. [7], where it is observed that, as $S$ increases, the number of liquid bridges increase as well. Beyond about $S = 0.07$, liquid bridges start to coalesce, with the coalesced liquid network exhibiting a percolation transition around $S = 0.2$. This value coincides very well with the value for $S$ at which we see the initial reduction in $d$, and at which the data collapse reaches its worst. This suggests that cohesion due to surface tension at air-liquid interfaces must be the primary mechanism by which the liquid contributes to stopping the projectile for small values of $S$. Presumably for $0.45 < S < 1$, the dominant capillary mechanism transitions from capillary action across liquid bridges to whatever mechanism enhances the stopping force at $S = 1$, which might explain the nonlinearity

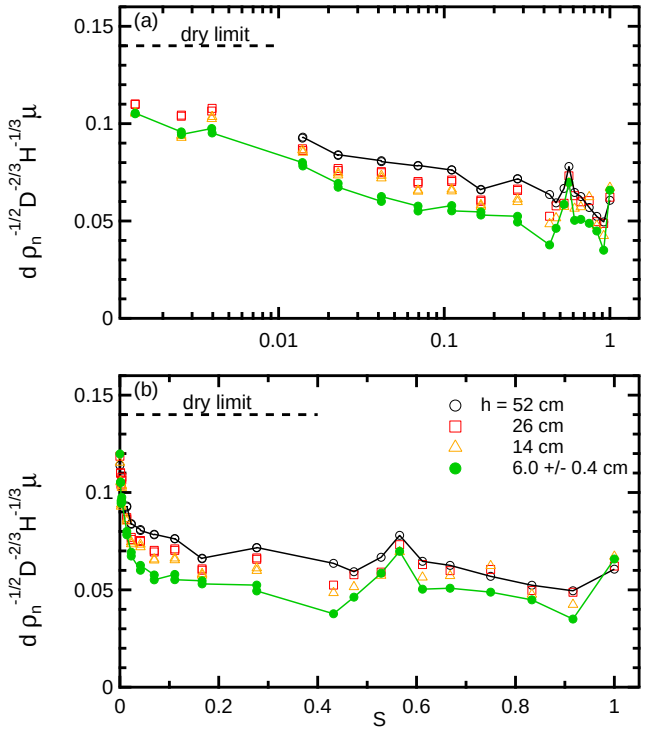


FIG. 3: (Color online) Penetration depth, $d$, normalized according to Eq. (1), plotted against liquid saturation for spheres of diameter 2.54 cm and density 0.68 g/mL, dropped into a bed of spherical glass beads wetted by oil, for various drop heights, $h$, as indicated by color. The data points for the largest and smallest drop heights are connected by solid lines to highlight variations in the quality of collapse.

of the data. Finally, as $S \to 1$, capillary action between individual grains must vanish as the amount of liquid-air interfacial area in the interior of the packing goes to zero. This is born out by the final increase in penetration depth, and the good agreement with the functional form of Eq. (1) at $S = 1$.

## IV. CONCLUSIONS

In conclusion, we find that the penetration depth, $d$, of a projectile impacting upon a granular packing is always reduced when an interstitial liquid is added to the packing. For fully liquid-saturated packings the functional dependence of $d$ on $\rho_n$, $D$, and $H$ is the same as for dry grains. The unchanged $H$- and $D$-dependence of the penetration depth reflect that the rate- and intruder size-dependence of the stopping force is the same as for the dry case, suggesting that the enhanced stopping force is not due to a viscous contribution. This interpretation is borne out by the fact that we measure deeper impacts for the more viscous fluid (oil). This result, along with the seemingly small contribution of fluid inertia, indicates that the enhanced stopping force is the consequence of a more complex mechanism, perhaps involving surface tension acting at the boundaries of the packing.

In contrast to the saturated case, for $0 < S < 1$, Eq. (1) no longer describes the functional dependence of $d$ on $H$. In fact, the $S$-dependence of penetration depth is strongly non-monotonic. Thus, while the depth-averaged stopping force exerted by a granular packing upon the projectile is enhanced by the presence of an interstitial fluid under all conditions, which is the dominant mechanism behind this enhancement must be dependent on $S$. The dramatic increase in stopping force for small amounts of liquid, $S < 0.2$ and subsequent $S$-independence tracks well with reports of the total area of liquid-air interfaces in the bulk [7], indicating that this initial enhancement of the stopping force must be due largely to capillary action across liquid bridges. We are not aware of any theoretical or structural data to compare to for $0.45 < S < 1$, but as $S \to 1$, capillary action between individual grains must vanish. Both the intervening non-linearities in penetration depth and the changes in functional form indicate that there is a complex evolution of the liquid conformation before the pores reach saturation.

In the future, either experimental data or theory describing the conformation of liquid in the pores could illuminate the complexity we observe in the impact dynamics for $0.45 < S < 1$. For all values of $S$, direct measurements of the stopping force and high-resolution position data taken *during* impact might enable us to determine the full form of the stopping force, mirroring the approach we have used to develop a working model for $S = 0$ [10, 13, 14, 20]. Also, while it is difficult to vary viscosity or surface tension independently, experiments with a broader variety of liquids would help to differentiate the roles of viscosity, density and surface tension. Lastly, to test the idea that dilatancy plays an important role at $S = 1$, high speed imaging of the packing surface during an impact may be sufficient. If not, tools like X-ray imaging could be used to directly measure the liquid fraction in situ.

### Acknowledgments

We would like to thank Jeremy Marston and Kerstin Nordstrom for helpful discussion. This work is supported by the National Science Foundation through grants MRSEC/DMR-1120901 and DMR-1305199.

[1] N. Mitarai and F. Nori, Advances in Physics **55**, 1 (2006).

[2] S. Strauch and S. Herminghaus, Soft Matter **8**, 8243

(2012).
[3] D. Hornbaker, R. Albert, I. Albert, A.-L. Barabasi, and P. Schiffer, Nature **387**, 765 (1997).
[4] F. Restagno, L. Bocquet, and E. Charlaix, Euro. Phys. J. E **14**, 177 (2004).
[5] S. Nowak, A. Samadani, and A. Kudrolli, Nature Physics **1**, 50 (2005).
[6] P. Pierrat and H. S. Caram, Powder Technology **91**, 83 (1997).
[7] M. Scheel, R. Seemann, M. Brinkmann, M. Di Michiel, A. Sheppard, and S. Herminghaus, J. Phys.: Cond. Matt. **20**, 494236 (2008).
[8] S. M. Iveson and N. W. Page, Powder Technology **152**, 79 (2005).
[9] J. C. Ruiz-Suarez, Rep. Prog. Phys. **76**, 6601 (2013).
[10] J. S. Uehara, M. A. Ambroso, R. P. Ojha, and D. J. Durian, Phys. Rev. Lett. **90**, 194301 (2003).
[11] M. A. Ambroso, C. R. Santore, A. R. Abate, and D. J. Durian, Phys. Rev. E **71**, 051305 (2005).
[12] E. L. Nelson, H. Katsuragi, P. Mayor, and D. J. Durian, Phys. Rev. Lett. **101**, 068001 (2008).
[13] L. S. Tsimring and D. Volfson, Powders & Grains **2**, 1215 (2005).
[14] T. A. Brzinski, P. Mayor, and D. J. Durian, Phys. Rev. Lett. **111**, 168002 (2013).
[15] H. Katsuragi and D. J. Durian, Phys. Rev. E **87**, 052208 (2013).
[16] J. O. Marston, I. U. Vakarelski, and S. T. Thoroddsen, Physical Review E **86**, 020301 (2012).
[17] K. Nordstrom, E. Lim, M. Harrington, and W. Losert, arXiv preprint (2013), 1304.6419.
[18] H. Takita and I. Sumita, Phys. Rev. E **88**, 022203 (2013).
[19] T. J. Wilson, C. R. Pfeifer, N. Mesyngier, and D. J. Durian, arXiv preprint (2013), 1307.2812.
[20] H. Katsuragi and D. J. Durian, Nature Physics **3**, 420 (2007).